QATNU Shutter Phase VII

Canonical Tensor Networks, Explicit Native Outgoing Traces, and the Quantum-to-Classical Controller Limit

Computational experiment report

19 June 2026

Abstract

This report closes the principal numerical bottleneck left by Phase VI and combines several previously separate shutter tests in one native smooth-boundary model. The earlier long-chain TEBD failure is traced to singular-value truncation outside a mixed-canonical gauge. A replacement center-moving canonical algorithm exhibits monotone bond-dimension convergence, exact small-system second-order time-step convergence, and stable autonomous scattering through 24 local square-root edge ladders. In the exact native chain, complete terminal-block algebras agree with an independently prescribed smooth-history reference to 7.95×10^{-5} at $N = 24$, while global and joint outgoing states remain distinguishable. An explicit right/left positive-frequency reduction and partial trace gives a resolved forward distribution with nonzero weight in every represented sector. For $N = 16$, the right and left marginal trace distances from the prescribed-history reference are 0.00402 and 0.00748, but the joint two-mode distance is 0.10191. Replacing the single controller by a collective controller of size M suppresses the joint-state discrepancy approximately as $M^{-0.940}$ and suppresses excess vacuum particle production as $M^{-1.005}$. The resulting interpretation is precise: the mean switching history controls far local observables, while quantum controller branches remain encoded in global field correlations.

Principal conclusion. The long-chain tensor-network failure was numerical rather than physical: noncanonical truncation was discarding the wrong singular values. The repaired solver converges and agrees across independent regulators. In the same native model, far local field algebras are governed mainly by the mean boundary history, whereas the controller's quantum branch structure survives in outgoing correlations. A collective controller recovers the prescribed classical switch with approximately $1/M$ corrections.

1 Scope and model

The field is one undoubled chain of native square-root edge ladders. In the low-occupation sector,

$$a|n\rangle = \sqrt{n}|n-1\rangle. \tag{1}$$

The open field Hamiltonian is quadratic in the associated quadratures. A finite central barrier is represented by the direct inter-edge bilinear

$$C = \eta\kappa q_\ell q_r. \tag{2}$$

Two ordinary matter qubits control the barrier through the standard frustration projector

$$F = \frac{I - Z_0 Z_1}{2}, \qquad F^2 = F. \tag{3}$$

The autonomous joint Hamiltonian is

$$H = I_m \otimes H_{\text{open}} + F \otimes C + \frac{\Omega}{2} X_0 \otimes I_e. \tag{4}$$

The initial matter state is the frustrated state $|01\rangle$, so the barrier begins closed. With $\Omega = \pi/T$, the free matter controller has

$$p^{\text{free}}_{\text{closed}}(t) = \cos^2\left(\frac{\pi t}{2T}\right). \tag{5}$$

Each exact run is generated by one fixed, time-independent Hamiltonian. The reference field state is generated independently under

$$H_{\text{ref}}(t) = H_{\text{open}} + p^{\text{free}}_{\text{closed}}(t) C. \tag{6}$$

This distinction is essential: no observable or outgoing mode is fitted by adjusting the reference switching law to the final autonomous field state.

The exact projected scattering family is summarized below.

N	T	$\mathcal{T}_{\text{auto}}$	$\mathcal{T}_{\text{open}}$	$\mathcal{T}_{\text{closed}}$	final P_{closed}
12	13.5056	0.80754477	0.95631842	0.10358853	0.15062560
16	18.0074	0.77889845	0.94006386	0.06691351	0.18000429
20	22.5093	0.76469400	0.92376612	0.05809335	0.19828564
24	27.0111	0.75974619	0.91907562	0.05239592	0.21059923

The largest packet-energy drift is 1.03×10^{-11}. Raising the global occupation cutoff from $n_{\max} = 4$ to 5 changes transmission by 0.244% at $N = 12$ and 0.232% at $N = 16$. Because the $n_{\max} = 4$ top shell is parity suppressed, the cutoff test uses the actual $4 \to 5$ change rather than the top-shell probability alone.

2 Canonical tensor-network repair

2.1 Why the earlier TEBD scan failed

The previous algorithm performed local SVD truncation when the state was not in mixed-canonical form. Those singular values were not the Schmidt spectrum across the cut, so the discarded-weight proxy was not a controlled error. Increasing the nominal bond dimension produced the nonmonotonic transmissions

$$0.56176, \quad 0.54873, \quad 0.50925, \quad 0.52326 \tag{7}$$

for $\chi = 32, 40, 48, 64$.

The repaired solver moves the orthogonality center with the sweep. A left-to-right split leaves the center on the right, a right-to-left split leaves it on the left, and every truncated SVD therefore acts on true Schmidt coefficients. Independent dense two- and three-site gate tests agree with direct contraction at approximately 4×10^{-15}.

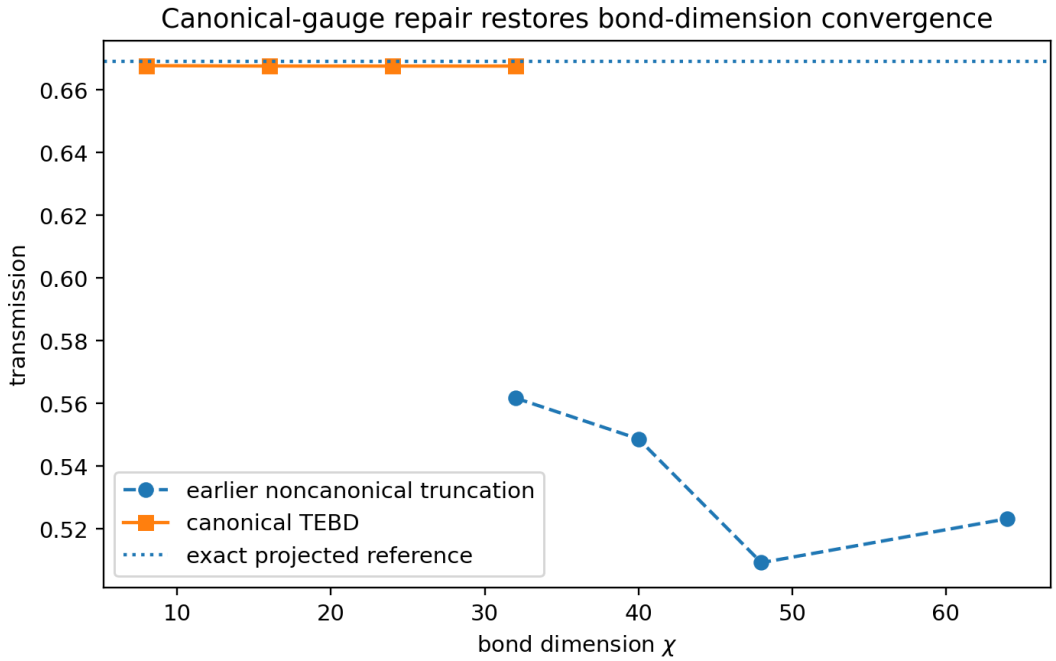

Figure 1: The earlier noncanonical truncation is nonmonotonic in bond dimension. The repaired mixed-canonical solver converges rapidly. The small residual offset from the projected reference at this fixed Δt is a time-step and local-dimension effect, not a bond-dimension effect.

At local dimension $d = 3$ and $\Delta t = 0.2$, the canonical transmissions are

χ	transmission	accumulated discarded weight
8	0.66774163	3.42×10^{-5}
16	0.66761123	4.23×10^{-7}
24	0.66761003	2.09×10^{-8}
32	0.66760608	2.34×10^{-9}

The final canonical residual is below 1.1×10^{-14}.

2.2 Exact time-step validation

A six-site, $d = 3$ benchmark with no bond truncation was compared directly with exact exponentiation.

Δt	packet fidelity^2	transmission error
0.200	0.9992421026	0.0223072595
0.100	0.9999553389	0.0055616461
0.050	0.9999972486	0.0013891662
0.025	0.9999998287	0.0003472089

The transmission error is linear in Δt^2 with $R^2 = 0.999999594$, and a direct log–log fit gives exponent 2.0018. The packet infidelity scales approximately as $\Delta t^{4.035}$, consistent with squaring a second-order state error.

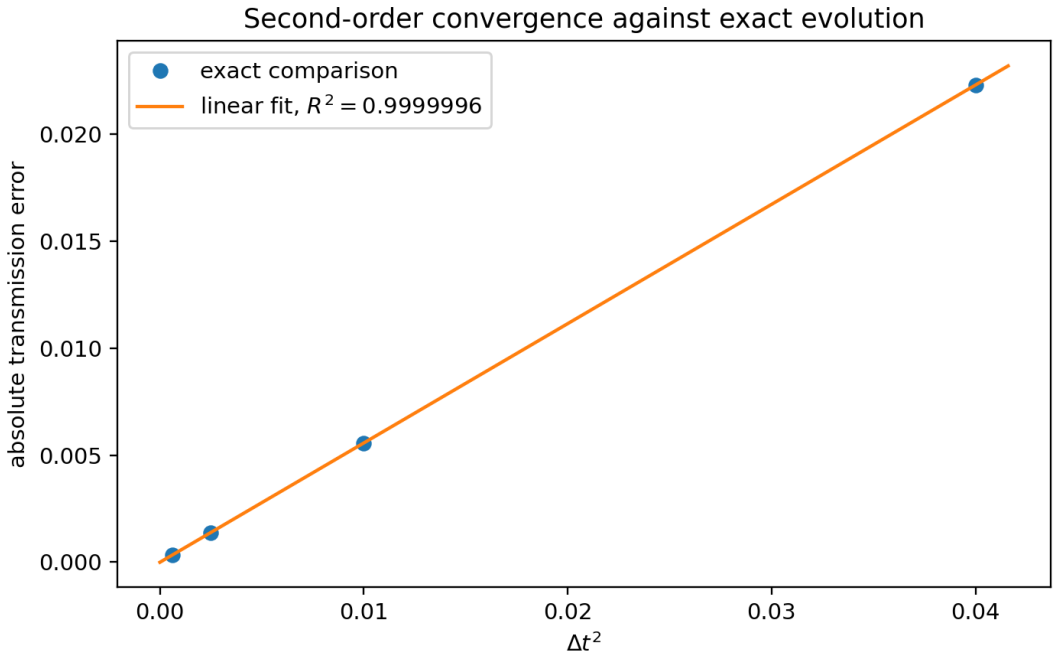

Figure 2: Exact small-system validation of the symmetric canonical TEBD step.

2.3 Local Fock dimension and long-chain propagation

For the 12-site benchmark, quadratic extrapolation in Δt^2 gives

local dimension d	$\Delta t \to 0$ transmission
3	0.67627333
4	0.66820117
5	0.66917870

The independent projected reference is 0.66907648. The $d = 5$ extrapolation differs by 1.0222×10^{-4} absolutely, or 1.53×10^{-4} relatively.

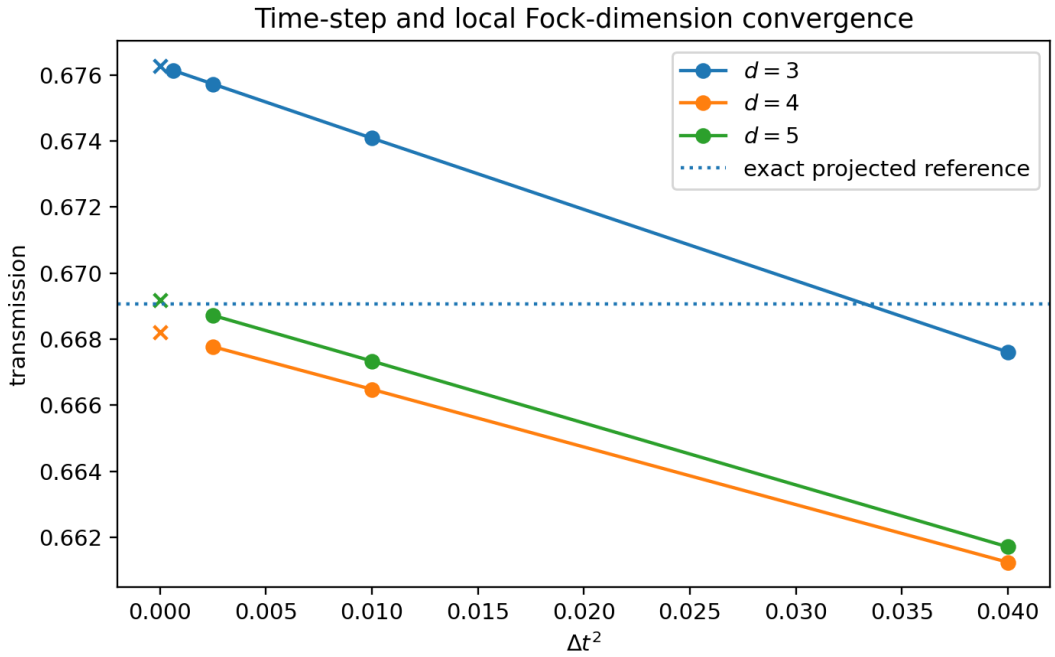

Figure 3: Joint time-step and local-Fock-dimension convergence. The crosses at $\Delta t = 0$ are quadratic extrapolations.

The repaired local-product solver now reaches 24 edge oscillators.

N	d	χ	MPS $\mathcal{T}$	projected $\mathcal{T}$	$\lvert\Delta\mathcal{T}\rvert$
12	3	24	0.81768628	0.80754477	0.01014151
12	4	32	0.80619247	0.80754477	0.00135230
16	3	24	0.78742550	0.77889845	0.00852704
16	4	32	0.77850911	0.77889845	0.00038934
20	3	24	0.77060753	0.76469400	0.00591352
24	3	24	0.76171489	0.75974619	0.00196870

All final canonical residuals are below 1.0×10^{-14}; the largest accumulated discarded weight is 1.14×10^{-7}.

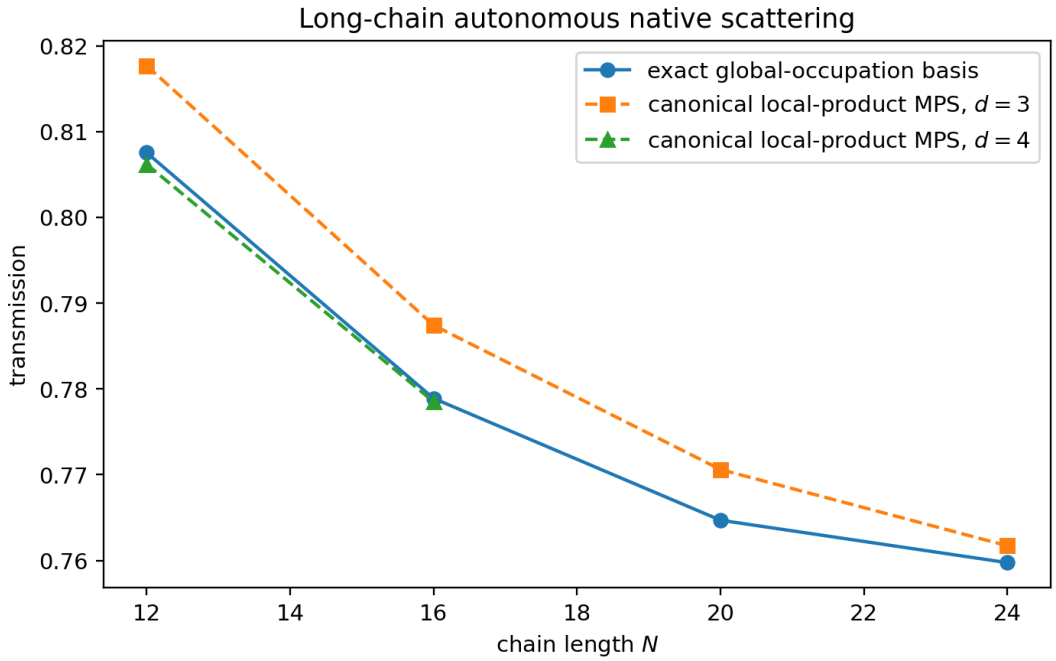

Figure 4: Exact projected and unrestricted local-product results for the same native smooth-shutter family. The $d = 4$ points provide the strongest regulator cross-check.

2.4 Exact entanglement and local-cutoff budgets

The exact 12-site projected trajectory has maximum packet entropy

$$S_{\max} = 0.69678335 \text{ nats} \tag{8}$$

and maximum exact Schmidt rank 112. To keep discarded Schmidt weight below 10^{-4}, 10^{-6}, and 10^{-8} on every cut requires only

$$\chi = 5, \quad 11, \quad 33. \tag{9}$$

The maximum local occupation tails are

$$P(n_j \geq 3) = 3.6383 \times 10^{-3}, \quad P(n_j \geq 4) = 2.8996 \times 10^{-5}, \quad P(n_j \geq 5) = 1.3611 \times 10^{-5}. \tag{10}$$

The former solver failure was therefore not caused by inaccessible entanglement or local occupation.

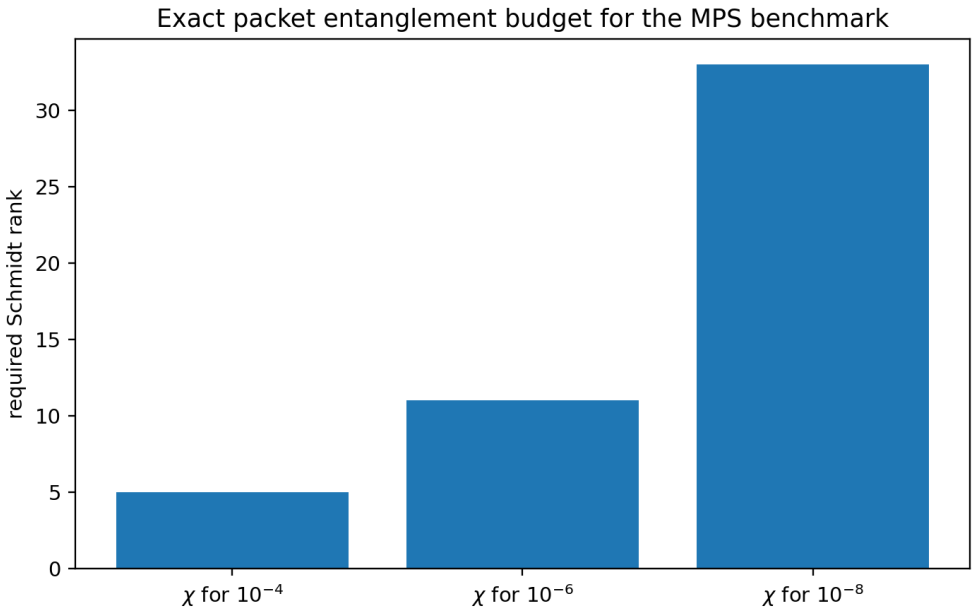

Figure 5: Exact Schmidt-rank budget for the packet benchmark.

3 Complete local observable algebras

For a native block A, the quantity

$$D_A = \frac{1}{2} \left\| \rho_A^{\mathrm{auto}} - \rho_A^{\mathrm{ref}} \right\|_1 \tag{11}$$

is the maximum statistical distinction over the complete local algebra, not a selected correlator set. For right terminal blocks, the three-site distances are

N	matched-history reference	static-open reference	improvement factor
12	0.00483808	0.04730125	9.78
16	0.00070901	0.01083477	15.28
20	0.00013725	0.00593360	43.23
24	0.00007947	0.00452968	57.00

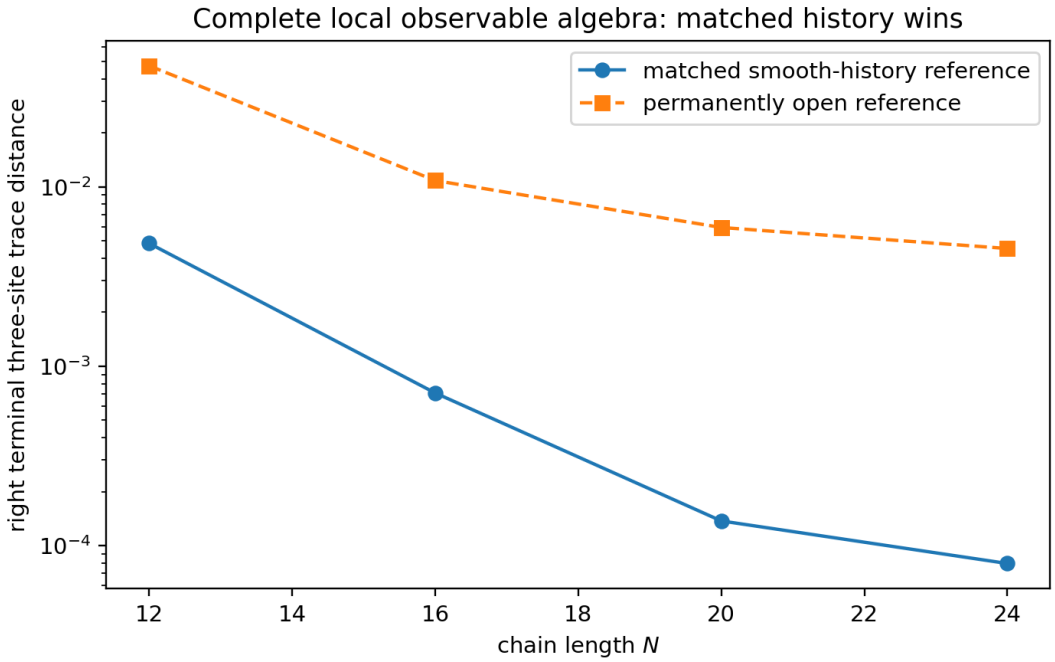

Figure 6: Complete right-terminal three-site algebra. Matching the smooth switching history is far more accurate than comparing with a permanently open chain.

At $N = 16$, the residual is concentrated near the central barrier. The maximum three-site distance anywhere is 0.0976836, while the complete terminal distance is 0.00070901.

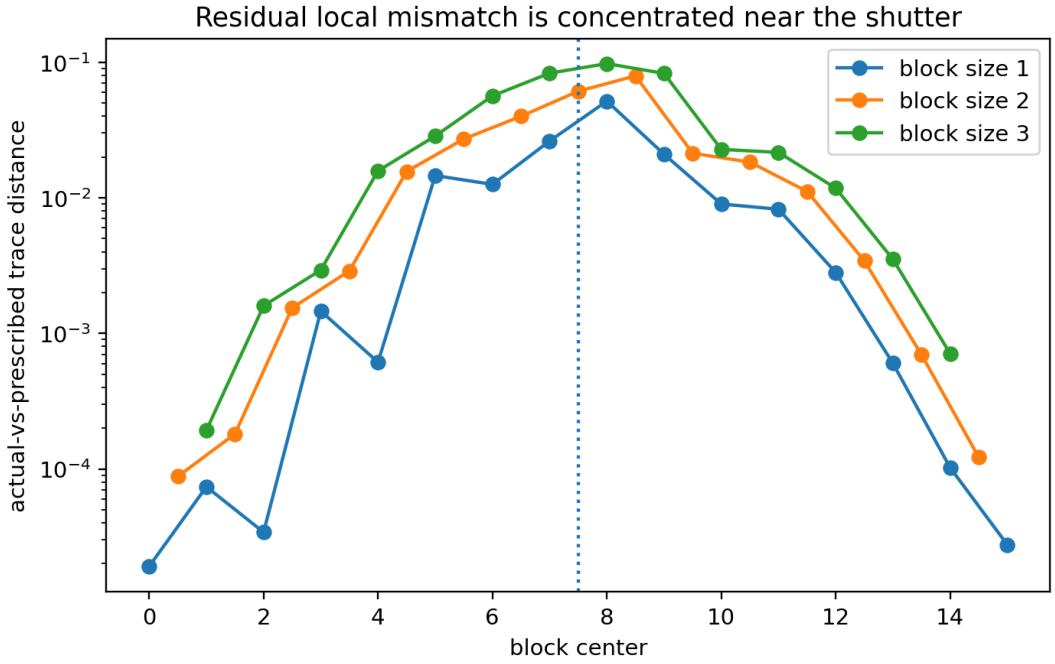

Figure 7: Spatial profile of the complete block-algebra distance at $N = 16$. The dotted line marks the central shutter.

The global packet-reference fidelity is 0.85206574, implying

$$0.0769259 \leq D_{\mathrm{global}} \leq 0.384622. \tag{12}$$

The global lower bound is more than 108 times the right-terminal three-site distance. The mismatch is therefore stored primarily in the switching region, the controller, and nonlocal correlations rather than in far local observables.

4 Explicit native outgoing partial trace

4.1 Regional positive-frequency modes

The leading packet-minus-vacuum natural orbital is found independently on the left and right spatial regions. Each orbital is projected into the open-chain positive-frequency basis, defining c_L and c_R. The finite two-mode density matrix is reconstructed with the normal-ordered vacuum projector and the left mode is traced explicitly:

$$\rho_R = \mathrm{Tr}_L\, \rho_{RL}. \tag{13}$$

The direct one-mode reconstruction agrees with the joint partial trace to 4.26×10^{-6} at $N = 16$ and 1.18×10^{-6} at $N = 24$.

For the unconditional $N = 16$ packet state,

n	$P_R(n)$	$P_L(n)$
0	0.517215952	0.876220414
1	0.482631166	0.123710842
2	1.21186×10^{-4}	5.44682×10^{-5}
3	2.38413×10^{-5}	9.36500×10^{-6}
4	7.85497×10^{-6}	4.91078×10^{-6}

Every represented forward sector is positive and

$$P_R(n \geq 2) = 1.52882 \times 10^{-4}. \tag{14}$$

The joint state has mutual information 0.15334327 nats and negativity 0.03807625.

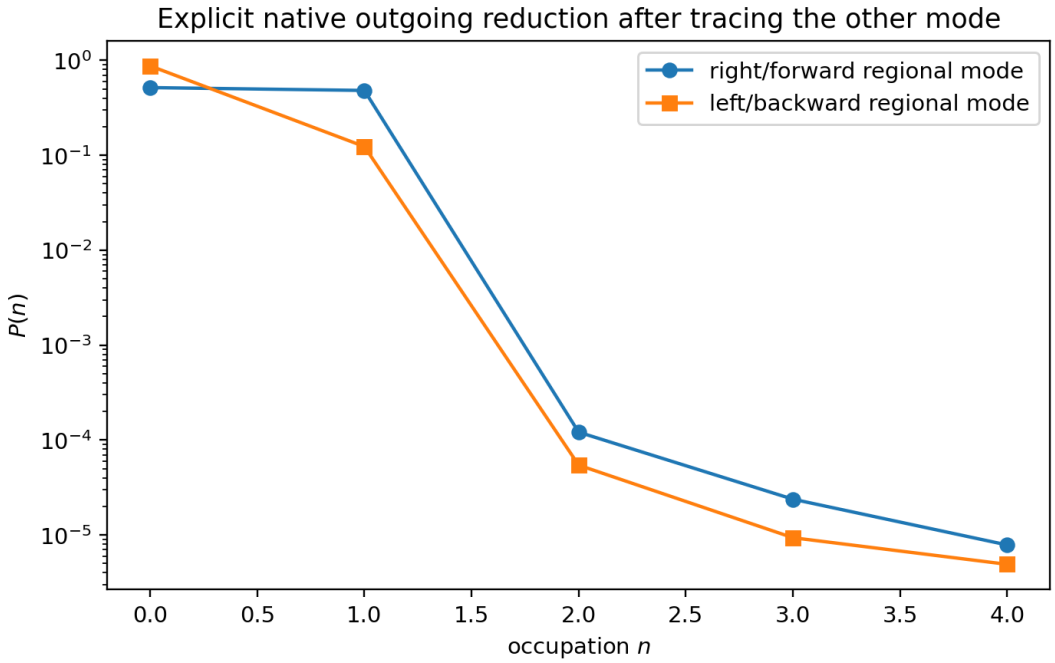

Figure 8: Explicit right/left regional-mode number distributions after tracing the other mode.

This is an actual partial trace in the autonomous native chain, but the finite Hilbert space establishes only support on every represented sector, not a literal infinite tail.

4.2 Independently fixed matched-history modes

A prescribed smooth-history reference is used to define the outgoing modes before examining the autonomous state. At $N = 16$,

$$D_R = 0.004022657, \qquad D_L = 0.007482813, \tag{15}$$

while

$$D_{RL} = 0.101909906. \tag{16}$$

The actual and reference right-mode profiles have overlap 0.998880216. The two-mode distance is about 25 times the right-marginal distance.

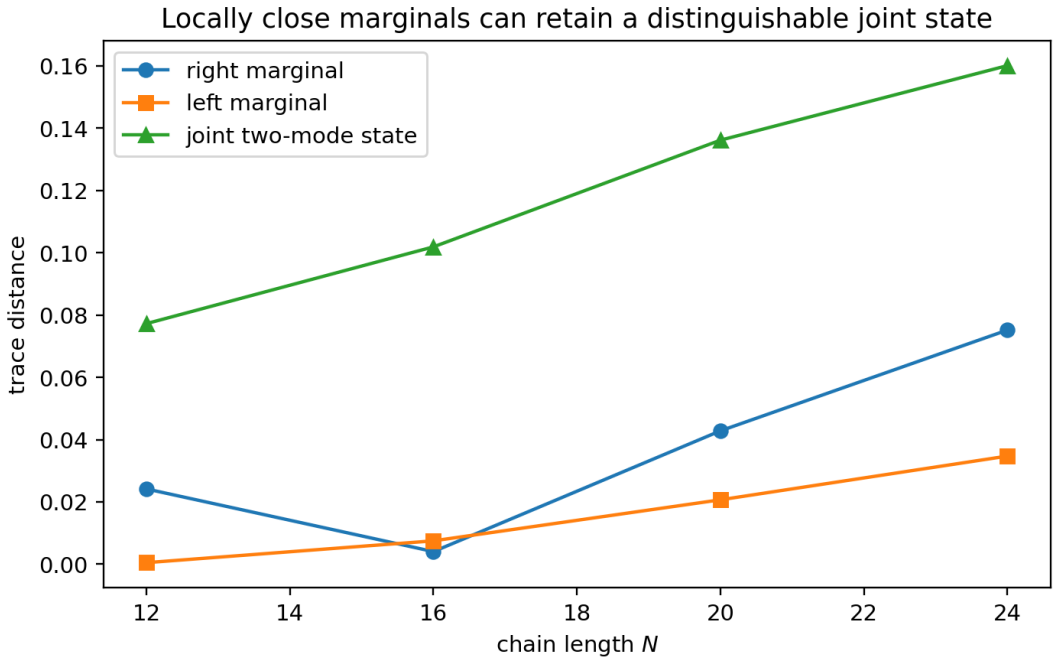

Figure 9: Marginal and joint trace distances in fixed modes defined by the prescribed smooth-history reference. The marginals can be locally close while the joint correlation state remains distinguishable.

The prescribed reference has mutual information 0.374510 nats and negativity 0.109718. Tracing the single quantum controller reduces the unconditional field values to 0.161927 nats and 0.0426733. Conditioning on the open matter branch restores 0.361258 nats and 0.102591. The final matter label therefore carries information about the outgoing correlation branch even when each local marginal is already close to the prescribed reference.

Here "left/backward" denotes the left regional outgoing positive-frequency mode. It is not yet a full asymptotic Moller scattering basis.

5 Residual branch and profile structure

In a small unrestricted local-product benchmark, the open-branch far-right residual from the mean-history reference is

$$D_{\text{residual}} = 0.08798731. \tag{17}$$

The dominant field Schmidt component has weight 0.96854598. The local distance between the actual mixed branch and that dominant component is only 0.00602765, while the dominant component itself remains 0.08197680 from the mean-history reference. The weighted dispersion among controller-basis conditioned local states is 0.17538997.

A symmetric two-profile ensemble preserving the same mean history lowers the distance to 0.07893627, an 11.5% improvement. These diagnostics are not additive decompositions, but they show that residual branch/history structure dominates local Schmidt mixing.

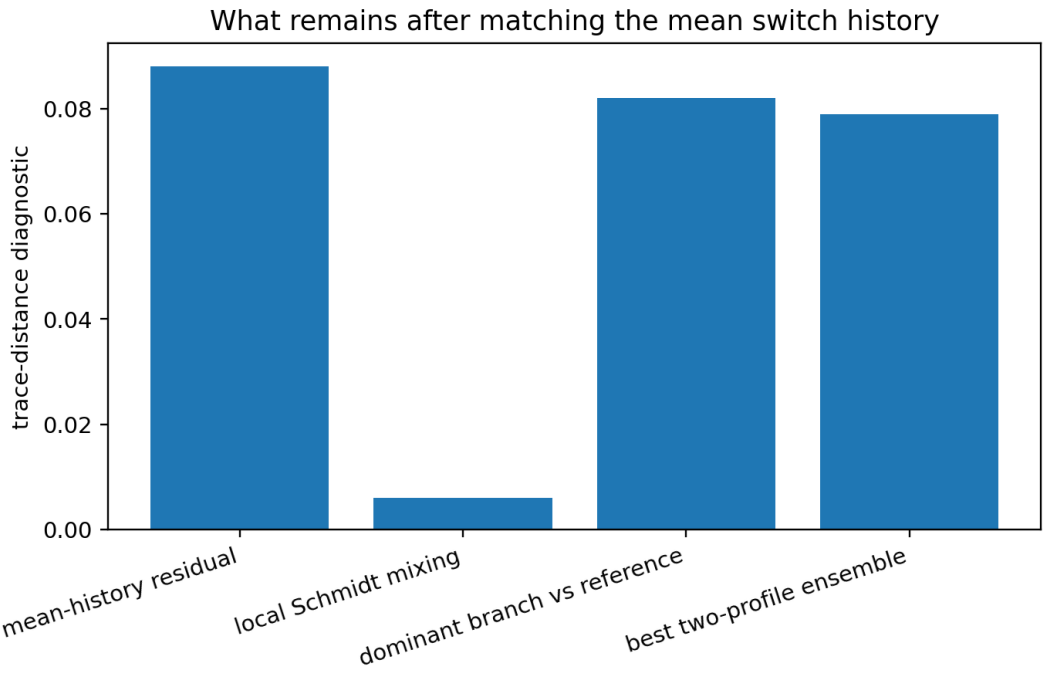

Figure 10: Nonadditive diagnostics of the residual after matching the mean switching profile.

6 Quantum-to-classical controller limit

6.1 Long-chain scattering

The controller is generalized to the symmetric sector of M identical two-level systems. The field couples to the collective closed fraction while the free collective rotation preserves the same mean profile in Eq. (5).

M	transmission	final P_{closed}	D_{block3}	D_{RL}	global infidelity
1	0.77889845	0.1800043	7.090×10^{-4}	0.1019099	0.1479343
2	0.78004029	0.0480819	3.764×10^{-4}	0.0533087	0.0863938
4	0.79226420	0.0122436	1.951×10^{-4}	0.0284561	0.0460954
8	0.80112173	0.0030761	9.950×10^{-5}	0.0147910	0.0237813
16	0.80632348	0.0007701	5.026×10^{-5}	0.0075515	0.0120695

The prescribed field-only transmission is 0.81209057.

For $M \geq 2$,

$$P_{\mathrm{closed}} \propto M^{-1.9886}, \quad D_{\mathrm{block3}} \propto M^{-0.9685}, \tag{18}$$

$$D_{RL} \propto M^{-0.9403}, \quad 1 - F_{\mathrm{global}} \propto M^{-0.9473}. \tag{19}$$

The latter three fits have $R^2 > 0.9994$.

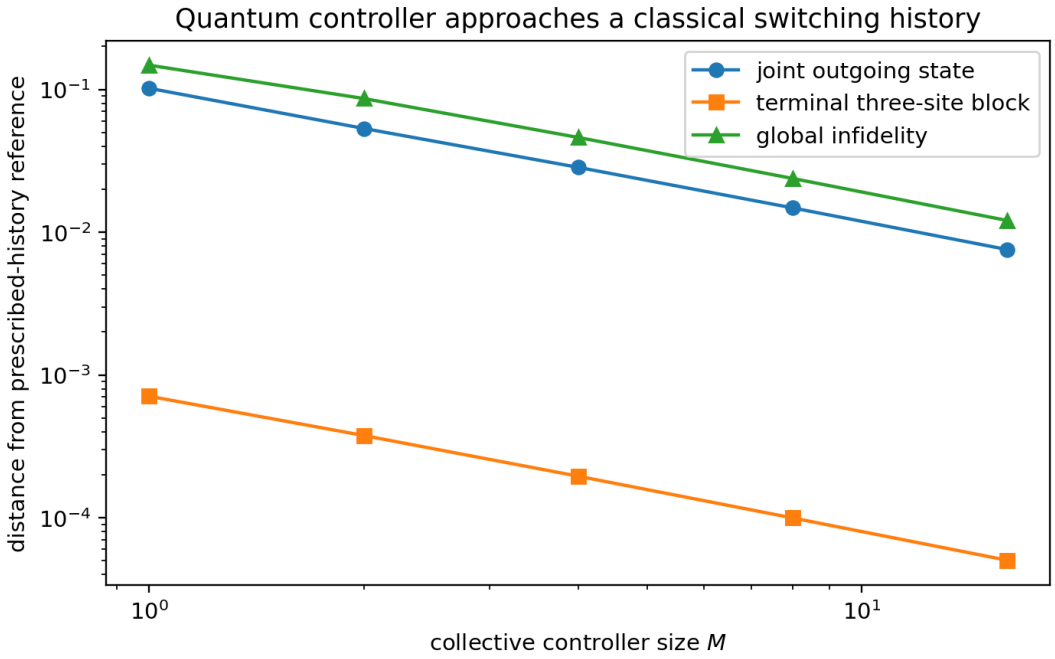

Figure 11: Collective-controller convergence toward the prescribed smooth-history field state.

6.2 Continuum-regulated vacuum production

At $N = 7$ and $n_{\max} = 8$, the autonomous particle-number excess above the prescribed native switch is

M	relative excess	final P_{closed}	controller entropy
1	0.3228419	0.0239221	0.0839026
2	0.1532985	0.0067155	0.0475414
4	0.0756841	0.0017256	0.0260195
8	0.0377454	4.3348×10^{-4}	0.0141979
16	0.0188657	1.0839×10^{-4}	0.0077238
32	0.0094382	2.7085×10^{-5}	0.0041839

The fit is

$$\frac{N_{\text{auto}} - N_{\text{prescribed}}}{N_{\text{prescribed}}} = 0.306043\, M^{-1.004760}, \qquad R^2 = 0.999946. \tag{20}$$

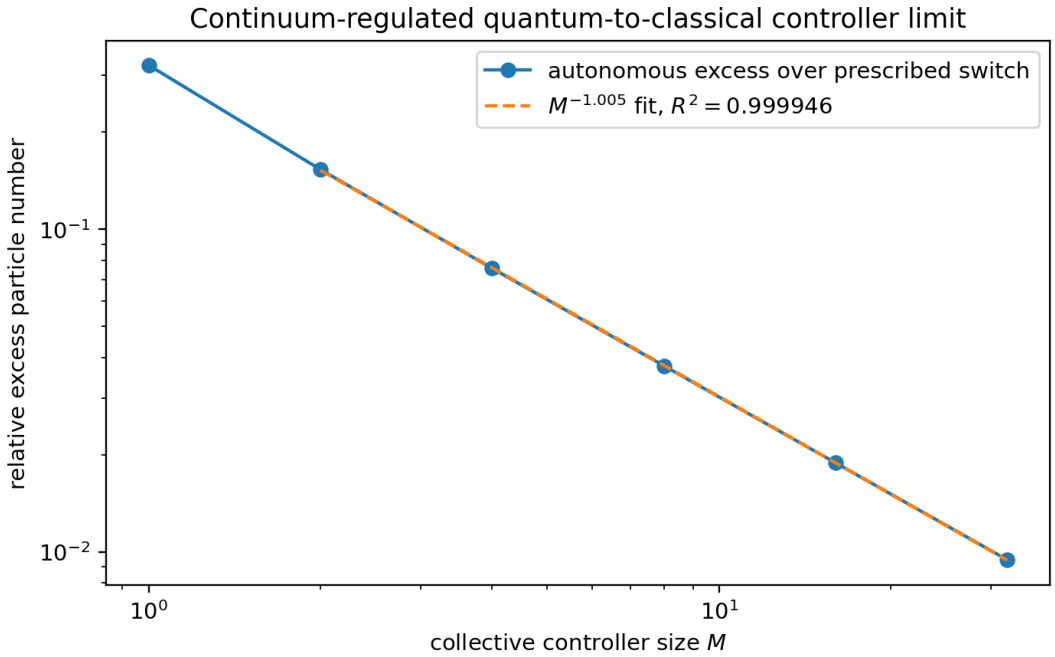

Figure 12: The additional radiation produced by quantum-controller fluctuations vanishes as approximately $1/M$.

For a single quantum controller, the controlled $n_{\max} = 10$ points give autonomous excesses of 26.01%, 32.35%, and 37.35% at $N = 5, 7, 9$. The prescribed native and Gaussian calculations agree within 0.16% or better at these points.

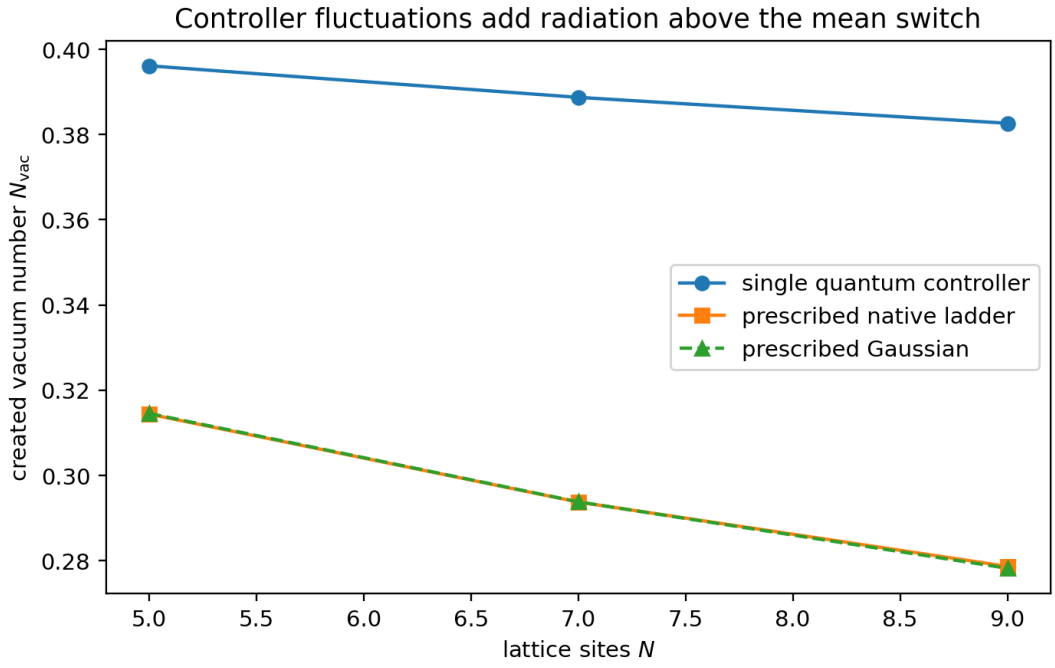

Figure 13: At fixed finite controller size, quantum branch fluctuations produce more vacuum excitation than the mean prescribed switch. Only cutoff-controlled $n_{\max} = 10$ points are shown.

The coefficient of this excess is model dependent. The robust result is the dynamic inequivalence of a finite quantum controller and its mean profile, together with a controlled collective limit.

7 What is established and what is not

Established finite-system result. A native square-root edge-ladder chain with a direct edge–edge bilinear and ordinary matter-frustration control supports stable autonomous smooth-shutter scattering in both exact projected and canonical local-product representations. Complete far-local algebras follow the independently prescribed mean boundary history, while the controller's quantum branch information remains in global and outgoing correlation structure. A collective controller recovers the prescribed classical switch with approximately $1/M$ corrections.

The following are not claimed:

- a derivation of electromagnetic $U(1)$ gauge structure from QATNU;
- a literal infinite photon-number tail in a finite native Hilbert space;
- a full asymptotic forward/backward scattering theorem on an infinite or absorbing chain;
- a simultaneous unrestricted-local-space, long-chain, spacing-to-zero limit for a finite quantum controller;
- universality of the finite-M excess-radiation coefficient;
- a full many-node matter/frustration network in which controller protection is dynamically derived.

8 Next decisive integrations

The highest-leverage next calculations are:

1. add absorbing leads or a substantially longer chain and construct fixed incoming/outgoing Moller wave packets rather than regional natural orbitals;
2. at every lattice spacing, converge local dimension and bond dimension before taking the spacing-to-zero limit, and repeat for several collective sizes M;
3. derive the $1/M$ correction analytically by expanding the collective controller around its spin-coherent trajectory;
4. repeat the two-packet connected-response experiment in the repaired long-chain solver and test its disappearance as M grows;
5. replace the active two-level controller sector by a spatial matter graph with penalties and leakage channels;
6. cross-check selected long-chain points with two-site TDVP or an independently implemented MPO-Krylov evolution.

Phase-VII synthesis. The mean boundary history determines far local outgoing observables, but a finite quantum controller is not equivalent to that mean history. Its branches and backaction remain visible in joint field correlations and additional radiation. The discrepancy becomes classical in a controlled collective limit.

Reproducibility

The accompanying bundle contains all source code, raw JSON and NPZ data, generated figures, the aggregate machine-readable summary, this report, a manuscript insertion, reproduction scripts, and SHA-256 checksums. The core solver tests can be regenerated independently of the expensive exact long-chain runs.